Blind deconvolution based equalizer for underwater acoustic communications

Salman I. Siddiqui*, Hefeng Dong

Department of Electronic Systems, Norwegian University of Science and Technology (NTNU), NO-7491 Trondheim, Norway.
{salman.siddiqui,hefeng.dong}@ntnu.no

Abstract

Reliable and efficient underwater acoustic communications are challenging problems because of complex underwater channel properties. With the recent advancements in underwater technologies, there is a need for a robust underwater communication system which can endure high data rate and optimize the use of resources like bandwidth and time. In this work, a blind deconvolution based equalizer is proposed, which uses the received signal to compute the channel impulse response estimates and equalizes the received signal using these channel impulse response estimates. The performance of the proposed system is tested with both simulated and real data. The real data were obtained during an experiment in September 2017 in TrondheimFjord. In the case of real data, the difference in performance in terms of mean square error between the proposed equalizer and the probe-based channel estimation equalizer is only 0.68 dB. This suggests that the proposed blind deconvolution technique can provide good channel estimates to equalize the underwater channel effects. In addition to that, it can save the resources allocated for the probe signal estimation.

1. Introduction

The underwater channel is a bounded medium and poses great challenges to underwater acoustic communications. The underwater channel is character-

*Corresponding author

ized as a dually spread channel in time and frequency. The time spreading of the channel is due to multiple paths from the surface and the bottom. The frequency spreading is caused by the source and/or receiver motion and the surface variations. The temporal and frequency spreading results in intersymbolic interference (ISI) and Doppler effects at the received signal respectively. To combat these complex channel variations, there is a need for a robust equalization system.

Due to recent developments in underwater acoustic systems, there is a growing need for efficient equalization techniques to combat the channel variations. Both coherent and non-coherent modulation schemes are used in the current underwater systems. In this work, the main focus will be on coherent schemes [1]. Coherent modulation schemes ensure high data rates but they are very sensitive to the time and frequency spreading of the underwater channel [2]. Different equalization techniques have been proposed in the literature for coherent schemes, including linear equalizers [3, 4] and direct sequence spread spectrum techniques [5, 6].

The performance of the underwater channel equalizers can be improved by using the spatial diversity which helps in reducing ISI [7]. In [8], the spatial diversity gain is combined with equalization gain to improve the performance of the underwater communication system. The equalization gain is mainly achieved by channel estimation. The channel estimate based equalizers have gained a lot of interest and different variants of these equalizers have been proposed, including time reversal equalizer [9, 10] and reduced complexity spatio-temporal equalizers [11]. One of the main challenges in the channel estimation based equalizers is the accuracy of the channel estimates. The effects of imperfect channel estimates have been studied in [12] and it shows that the performance degrades significantly in the presence of channel variations like surface motion. Some improved versions of these equalizers are proposed to update the channel impulse response (IR) estimates [12, 13, 14].

In addition to the accuracy of the channel IR, the underwater channel varies rapidly with time. To estimate these temporal channel variations, probe signals

need to be transmitted frequently which requires significant additional resources like bandwidth and time. In some cases of offshore underwater applications, it is impossible to get channel IR estimates. For all these underwater applications, there is a need for a blind channel estimation technique which can save the additional bandwidth and battery time and also provide good channel IR estimates.

In this paper, a blind deconvolution based equalizer is proposed. Blind deconvolution refers to the process of getting both the channel estimates and the source signal from the array-recorded signal. Different techniques have been proposed in the literature for blind deconvolution for underwater applications including time-frequency analysis [15], least-square criterion [16], and multiple convolutions [17]. In this work, artificial time reversal (ATR) technique proposed in [18] is used for blind deconvolution. ATR is based on the stable features of the lower order acoustic normal modes and on a receiving array with sufficient elements and aperture. In the ATR-based system, the channel IR estimates are obtained by applying a weighting functions on the received data signal.

In this paper, the ATR technique is used for designing an equalizer for the underwater communication system. It computes the channel IR estimate from the received information signal and uses this channel IR estimate to equalize the effects of the channel. The quality of the channel IR estimates varies depending on the weighting technique and it also affects the performance of the communication system. Three weighting functions are tested in this paper. These weighting functions are proposed in [18, 19]. In [19], the ATR based technique is used for source localization. The performance of the proposed system is compared with a known channel case in terms of the mean square error (MSE) and bit error rate (BER). The known channel case refers to the conventional time reversal system in which the channel IR estimate is obtained from the probe signal. The proposed system is tested with simulated as well as real data. The real data were obtained during the experiment in TrondheimFjord in September 2017. The results have shown that the proposed system provides good performance in terms of MSE and BER. In addition to that, the ATR system only

requires the received signal to compute the channel IR estimate. Hence, it saves the resources allocated for channel IR estimation. The main contributions of this work are; 1) To design a communication system based on blind deconvolution technique to combat the channel variations, 2) To study the performance of different ATR-based channel estimation techniques on the underwater communication system.

The paper is organized as follows. Section 2 describes the theoretical background. Section 3 discusses the receiver structure. Section 4 presents the results and observations for simulated as well as the real data cases. Section 5 provides the conclusions.

2. Theoretical Background

This section presents the mathematical formulation of the blind deconvolution technique. The blind deconvolution is based on the ATR technique. Consider a point source emitting a signal $s(t)$. All the formulation is done in the frequency domain so the Fourier transformed $S(\omega)$ is given by

$$S(\omega) = |S(\omega)|e^{i\theta_s(\omega)} \tag{1}$$

where ω is the angular frequency and $\theta_s(\omega)$ is the phase of the transmitted signal as a function of frequency. The transmitted signal passes through the channel and reaches the receiver array having N elements. The received signal at the j^{th} element is described by $R_j(\omega)$

$$R_j(\omega) = G(r_j, r_s, \omega)S(\omega) \tag{2}$$

where $G(r_j, r_s, \omega)$ is the channel IR between the source position r_s and receiver position r_j at the frequency ω. The main advantage of ATR is that it uses only the received signal at each array element to estimate the channel IR. These channel IR estimates are combined with the received signal in a maximum ratio combiner to obtain the output of the equalizer. The performance of the communication system relies on the channel IR estimation. The equalizer output

$Z(\omega)$ is given by

$$Z(\omega) = \sum_{j=1}^{N} \hat{G}^{*}(r_j, r_s, \omega) \cdot G(r_j, r_s, \omega) \cdot S(\omega) \tag{3}$$

where $Z(\omega)$ is the output of the maximal ratio combiner which selects the optimal value based on the maximum power. $\hat{G}(r_j, r_s, \omega)$ is the channel IR estimate and "$*$" denotes the conjugate operation.

According to ATR technique, the channel IR estimates are given by [18]

$$\hat{G}(r_j, r_s, \omega) = \frac{R_j(\omega) e^{-i\alpha(\omega)}}{\sqrt{\sum_{k=1}^{N} |R_k(\omega)|^2}} \tag{4}$$

where

$$\alpha(\omega) = \arg\left(\sum_{j=1}^{N} W_j R_j(\omega) \right) \tag{5}$$

In (5), W_j is the weight for the j^{th} element of the array. Different weighting functions are used in this paper. Using the value of $R_j(\omega)$ from (2) in (4), the estimated channel IR is given by

$$\hat{G}(r_j, r_s, \omega) = \frac{G(r_j, r_s, \omega) e^{-i\alpha(\omega)} e^{i\theta_s(\omega)}}{\sqrt{\sum_{k=1}^{N} |G(r_k, r_s, \omega)|^2}} \tag{6}$$

The optimal value of $\alpha(\omega)$ should cancel the phase term $\theta_s(\omega)$ or the remainder should be a linear function of frequency in the form of $a + b\omega$ which will only result in a shift in time.

In order to explain the weight functions, the expression for $\alpha(\omega)$ in (5) is studied in more detail. Inserting (2) into (5), $\alpha(\omega)$ becomes

$$\alpha(\omega) = \arg\left(\sum_{j=1}^{N} W_j S(\omega) G(r_j, r_s, \omega) e^{i\theta_s(\omega)} \right) \tag{7}$$

By expanding $G(r_j, r_s, \omega)$ using normal mode model [20],

$$\alpha(\omega) = \arg\left(\sum_{j=1}^{N} W_j S(\omega) e^{i\theta_s(\omega)} \frac{e^{-i\pi/4}}{\rho(z)\sqrt{8\pi}} \sum_{m} \frac{\Phi_m(z_s)\Phi_m(z_j)}{\sqrt{k_m(\omega) r_j}} e^{ik_m(\omega) r_j} \right) \tag{8}$$

where Φ_m and k_m are the mode shape and wavenumber for the m^{th} mode respectively and $\rho(z)$ is the density at depth z. The optimal weights W_j should be such that it cancels the mode shape $\Phi_m(z_j)$, which will simplify (8) to

$$\alpha(\omega) \approx k_n(\omega)R + \theta_s(\omega) - \pi/4 \tag{9}$$

where R is the distance between the source and the receiver array. If the cutoff frequency of the n^{th} mode is well below the frequencies of interest, the phase speed c_n will be independent of frequency and $k_n(\omega)R = \omega R/c_n$ [18]. Using this value of $\alpha(\omega)$ in (6), the channel IR estimate is obtained with an extra term $\omega R/c_n$ which is a linear function of frequency and produces a shift in the time domain. These time-shifted channel IR estimates are used to equalize the channel effects.

The main objective of the weighting function is to cancel the $\Phi_m(z_j)$ term which is achieved by the mode orthogonality principle

$$\sum_{j=1}^{N} \frac{\Phi_m(z_j)\Phi_n(z_j)}{\rho(z_j)} \approx \delta_{mn} \tag{10}$$

where W_j corresponds to $\Phi_n(z_j)$. The efficiency of the ATR based technique relies on weighting function and how it satisfies (10). The limitation of a densely populated array is also to ensure this condition.

In this paper, three types of weighting functions are used. In the first two types of weighting functions, constant weights are applied to each array element. In "array weights 1" all the weights of the array elements are set to +1. In "array weights 2", the weights of the first half of the array elements are set to +1 while the weights for the rest of the elements are set to −1. The third type of weighting function is based on beamforming (BF) technique. In the BF-based technique, the weight of each array element is computed by

$$W_j = \exp\{-i\omega\tau(\theta_k, z_j)\} \tag{11}$$

where $\tau(\theta_k, z_j)$ is the delay applied to each array element and it is a function of the BF angle θ_k and k is the index for the BF angle. In this case, plane ray

beamforming is used

$$\tau(\theta_k, z_j) = (j-1)(d/\bar{c})\ \sin\theta_k \tag{12}$$

where d is the spacing between the array elements and $\bar{c}$ is the mean sound speed profile (SSP). The optimal weight is obtained as a function of θ_k based on the maximum output power $Z(\omega)$ as given in (3).

In order to explain the concept of the weighting function and how the weighting functions help in providing better channel IR estimates, a simulated example is presented. In this simulation scenario, a waveguide of 200 m depth is considered and source and receiver array is located at 30 m depth. The receiver array contains 8 elements from 30 m - 37 m depth with 1 m spacing between each element. Using this geometry in KRAKEN [21], the modes shape functions of first 26 modes are computed. Using each of this mode shape function as a weight function $\Phi_n(z)$ in (10), the performance of the system is computed in terms of MSE and shown in Fig. 1 (a). Fig. 1 (a) shows that mode number 5, 11, 17 and 23 give the best performance. The optimal weighting function should enhance these modes and suppress the rest of the modes.

Fig. 1 (b) shows the sum of the weighted-mode shapes along the depths which is represented by (10). For comparison, the best BF weights are presented here which gives the maximum output power in (3). All three array weighting techniques give different weights to each mode. Fig. 1 (c) shows the product of Fig. 1 (a) and (b). The "array weights 2" does not give larger weights to lower order modes but enhances the higher order modes by giving them bigger weights. The "array weights 1" and "BF weights" have similar performance for lower order modes but the "BF weights" outperforms the "array weights 1" by suppressing the modes 13, 20 and 26, which have worst performance in terms of MSE.

Fig. 2 shows the channel IR estimates for the constant SSP at the fourth array element at 33 m depth. These channel IRs are obtained from the received signal by applying different weighting techniques according to (4). For comparison, the actual channel IR is presented in Fig. 2 (d) which is obtained from the model.

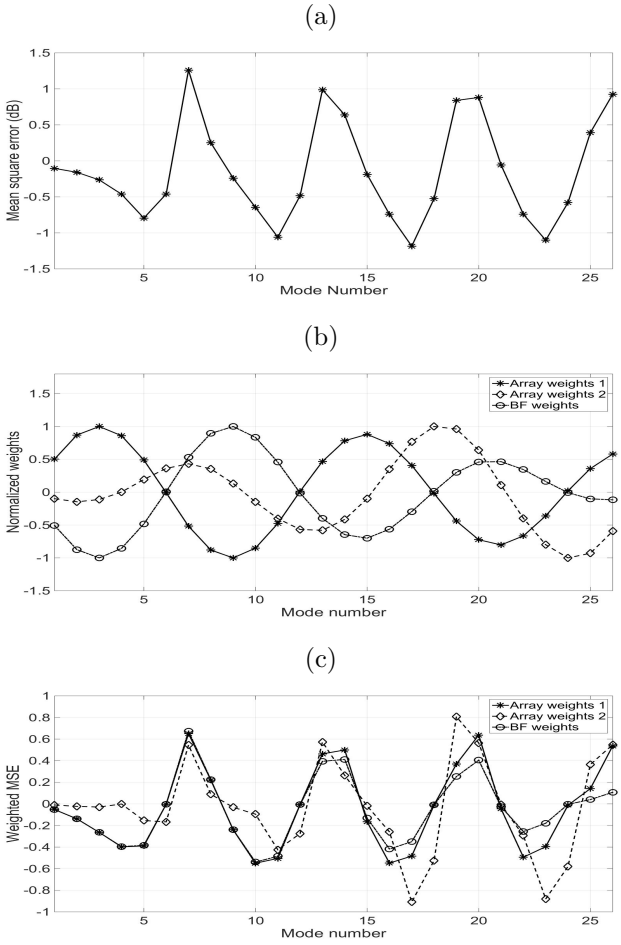

Figure 1: Using the simulated scenario with constant SSP, (a) Performance in terms of MSE for each mode shape function used as weight function Φ_n in (10), (b) shows how different weighting techniques enhance some modes and suppress other modes. The continuous line represents "array weights 1", dashed line represents "array weights 2" and the dotted line represents "BF weights", (c) Product of the MSE and mode weights for different weight functions.

In the case of BF weights, only the optimal channel IR is presented which gives the maximum output power. There are differences between the channel IR estimates obtained by ATR and the channel IR estimate from the model. These mismatches result in the degradation in the performance of the system.

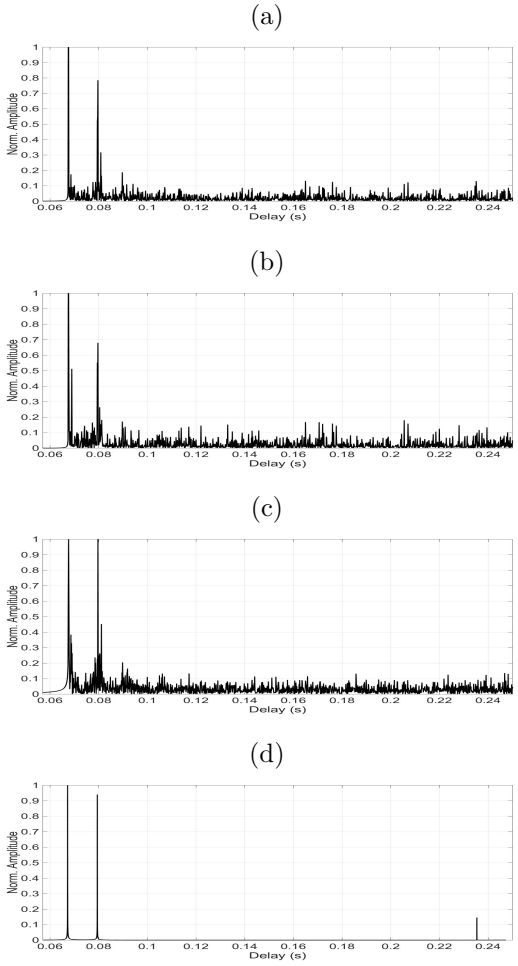

Figure 2: Channel IR estimates obtained for the simulation case of constant SSP at the fourth array element at 33 m depth. a) Channel IR obtained by "array weights 1", b) Channel IR obtained by "array weights 2", c) Channel IR obtained by "BF weights", d) Actual channel IR obtained by the model.

3. Receiver structure

This section explains the receiver structure of the proposed communication system. Fig. 3 shows the block diagram of the proposed system. The block diagram is derived from the passive time reversal system with the addition of the weight function block which is represented by $e^{-i\alpha(\omega)}$. All the operations are

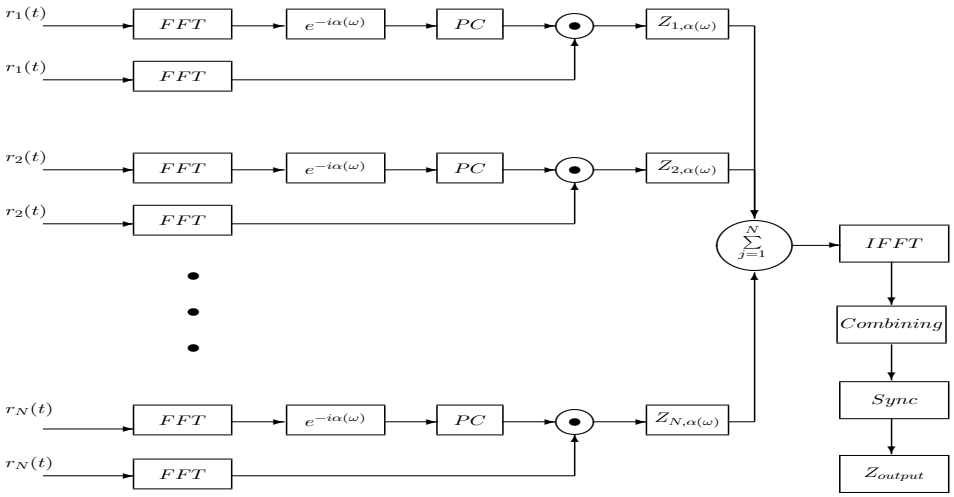

Figure 3: Block diagram of the proposed system.

performed in the frequency domain, therefore, a Fourier transform is applied to the received signal $r(t)$. The Fourier-transformed signal is fed to the weighting function block which provides the channel IR estimate. The PC block performs the phase conjugation. The phase-conjugated channel IR estimate is combined with the received signal and summed to give the output $Z(\omega)$ as given in (3). The block diagram presented in Fig. 3 is generalized for different types of weighting functions. In the case of constant weights for each array element, the output $Z(\omega)$ is a single vector while in case of BF-based weighting technique the output $Z(\omega)$ is a function of the BF angle. The "combining" block selects the optimal angle based on the maximum output power.

During data processing, the information bits are divided into blocks of 0.25 s and it is assumed that the channel is constant during this time. In the case of a BF-based system, the *combining* block works in two steps. In the first step, it splits the output into blocks and selects the optimum angle based on (3) for each block. In the next step, it selects the maximum power from all blocks and the corresponding BF angle. This BF angle is used for computing the channel IR estimates. The output of the combining block goes to the *sync* block.

The *sync* block performs two operations. Firstly, it is shown in section 2 that the weighting function produces a time shift. The *sync* block synchronizes the output with the known M-sequence, which is inserted at the start of the data signal. Secondly, using the same known M-sequence the phase correction is also performed. After *sync* block, the final output Z_{output} is obtained.

4. Results and Observations

In this section, the results and observations are presented. The performance of the proposed algorithm is tested with simulated as well as real data. The simulated environment is obtained from Time Variable Acoustic Propagation Model (TVAPM) [22]. The specifications of the transmitted signals are shown in table 1. During the experiment, linear frequency modulated (LFM) signals are transmitted as probe signal for channel IR estimation and data signal contains information bits. The same signal specifications are used for both simulations and experiment.

The performance comparison is presented between three weighting techniques and the known channel IR case. In the "known channel" case, the exact channel IR estimates are used and this case is presented here to show the best performance. In the simulated case, the channel IR estimates are obtained from TVAPM. In the case of real data, the channel IR estimates are obtained from the probe signal. The "known channel" case is equivalent to the conventional time reversal equalizer.

4.1. Simulated case

In the simulated scenario, both the source and receiver are considered static. The source is set at 30 m depth and 8-element receiver array is located between 30 m - 37 m depth with the first element at 30 m depth and the spacing of 1 m between each element. The water depth is 200 m, the source-receiver range

Table 1: Signal Specifications

Central Frequency (Hz)	8500
Sampling Frequency (Hz)	44100
Frequency band Data (Hz)	7000 - 10000
Data rate (bits/s)	2000
Modulation	BPSK
Frequency band LFM (Hz)	6320 - 10680
Time one LFM (s)	0.1
Silence Time (s)	0.2

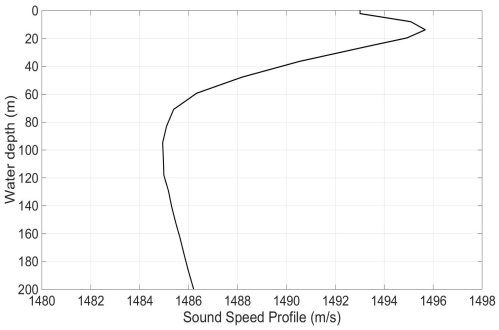

Figure 4: SSP obtained during an experiment in the TrondheimFjord in September 2017.

is 100 m and the flat bottom is considered. Two types of sound speed profiles (SSPs) are used. One is a constant SSP along depth and the second is a SSP obtained during the experiment in Sept. 2017 which is shown in Fig. 4. Fig. 5 shows the characteristics of the channel for the case of constant SSP. Fig. 5 (a) shows the arrival pattern at each element of the receiver array. The first arrival is the direct arrival because it arrives at all the receiver elements at the same time. The second arrival is the surface reflected arrival because it arrives first at the top element of the receiver. Fig. 5 (b) shows the beamforming results. The negative angles represent the arrival from the surface while the positive angles represent the arrival from the bottom. The first arrival reaches the receiver array at -2^o and the second arrival reaches the receiver array at -32^o.

Fig. 6 (a) shows the performance comparison in terms of MSE for different weighting techniques in case of constant SSP. The performances in terms of MSE of the constant array weighting techniques are -0.27 dB and -1.09 dB respectively. The better performance for the "array weights 2" can be explained from Fig. 1 because "array weights 2" gives larger weights to modes 17 and 23 which give good performance in terms of MSE. The BF-based weighting technique gives 2.3 dB and 1.4 dB gain in terms of MSE as compared to "array weights 1" and "array weights 2" respectively. The optimal BF weights are selected based on the maximum output power from all time slots. The dotted line shows the performance of the system in the case of perfect knowledge of the channel which is the ideal case. The BF-based weighting function case is outperformed by the ideal case by only 1.3 dB. This degradation in the performance is due to channel IR estimation error which can be seen from Fig. 2 (c) and (d). Fig. 6 (b) shows the performance comparison in terms of BER in case of constant SSP. The BER is calculated for a time slot of 0.25 s which contains 500 information bits. The "array weights 1" and "array weights 2" give a mean BER of 0.17 and 0.14. The BERs for "BF weights " and "known channel" are 0.089 and 0.104 where the BF-based weighting technique gives a gain of 1.5%.

Fig. 7 (a) shows the arrival pattern at each element of the receiver array for the

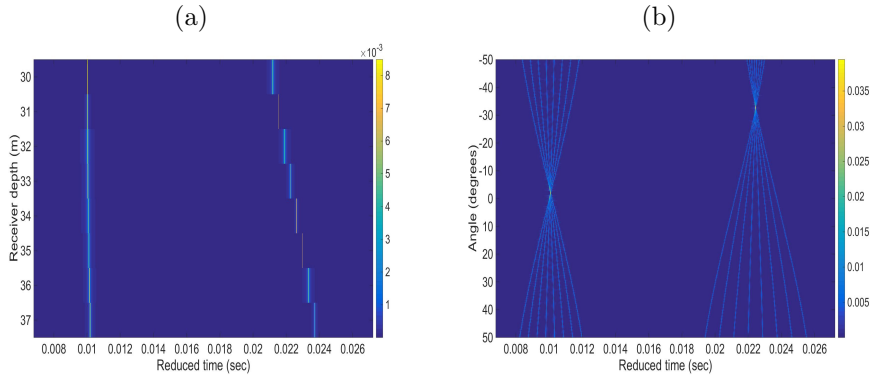

Figure 5: Characteristics of the channel for the case of constant SSP. (a) The channel IR estimates along the receiver array, b) The beamforming results showing the angle of arrival.

(a)

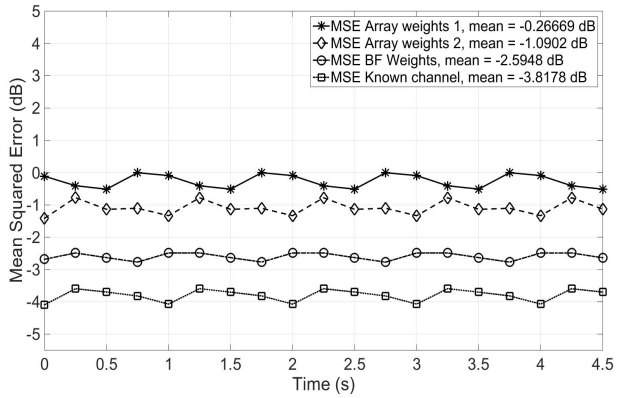

(b)

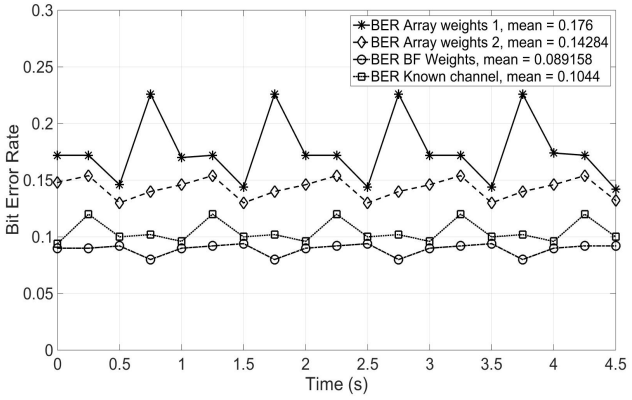

Figure 6: Performance comparison of different weighting function as a function of time for static source and receiver and constant SSP. (a) Performance in terms of MSE, (b) Performance in terms of BER

depth varying SSP. Similar arrival pattern is observed in this case. Two arrivals reach the receiver array. The first one is the direct arrival and the second is the surface-reflected arrival. Fig. 5 (b) shows the beamforming results. The first arrival reaches the receiver array at -2^o and the second arrival reaches the receiver array at -32^o.

Fig. 8 (a) shows the performance comparison when the depth varying SSP is used. There is a sharp gradient between 30 - 37 m depth in the SSP where

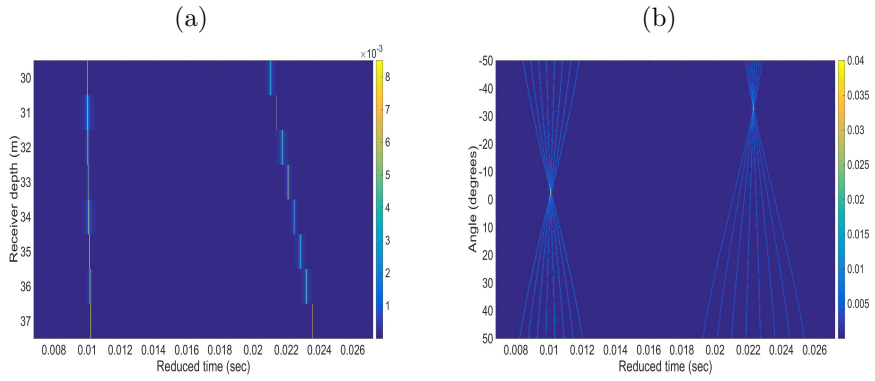

Figure 7: Characteristics of the channel for the case of depth varying SSP. (a) The channel IR estimates along the receiver array, b) The beamforming results showing the angle of arrival.

the array elements are located. The performance in terms of MSE of the two array weighting techniques is 0.7 dB and -0.04 dB. The BF-based weighting technique gives a gain of 3.809 dB and 3 dB in terms of MSE as compared to "array weights 1" and "array weights 2" respectively. Fig. 8 (b) shows the performance comparison in terms of BER in the case of depth varying SSP. The "array weights 1" and "array weights 2" give a mean BER of 0.47 and 0.38. The BER for "BF weights " and "known channel" are 0.166 and 0.107 where the BF-based weighting technique is outperformed by "known channel" case by 5.9%.

Comparing Fig. 6 and Fig. 8, the performance of constant weighting techniques degrades in case of depth varying SSP. In the case of "array weights 1" and "array weights 2', the performance degradation is 0.97 dB and 1.05 dB respectively, while the performance of BF-based weighting technique improves by 0.51 dB. The degradation in the performance for constant array weights is because of the channel IR estimation errors. The BF-based weighting technique performs better as compared to constant weighting technique because it provides better channel IR estimates.

(a)

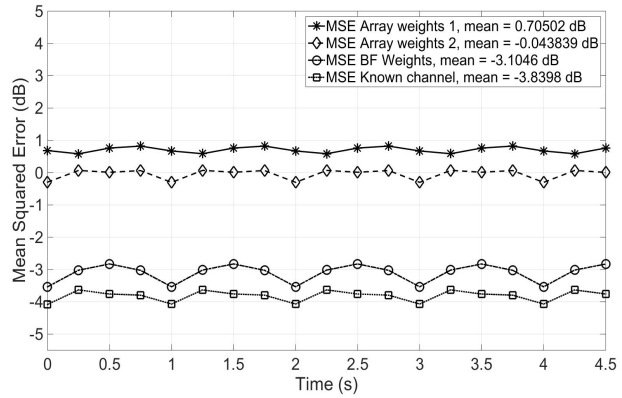

(b)

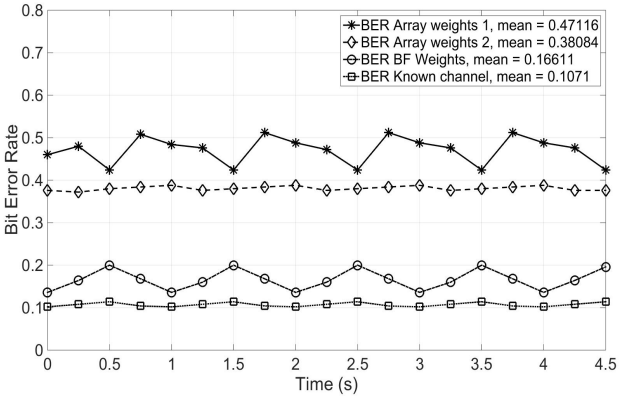

Figure 8: Performance comparison of different weighting function as a function of time for static source and receiver and depth varying SSP. (a) Performance in terms of MSE, (b) Performance in terms of BER

4.2. Real data case

In this section, the results for the real data are presented. The data were obtained from an experiment in the TrondheimFjord on 29 September 2017. Fig. 9 shows the bathymetry of the area of experiment and the source and receiver positions. The water depths at the source and receiver positions were 150 m and 200 m respectively. The source-receiver range was 480 m. The receiver array was deployed at 50 m depth. The receiver array consisted of 8 elements

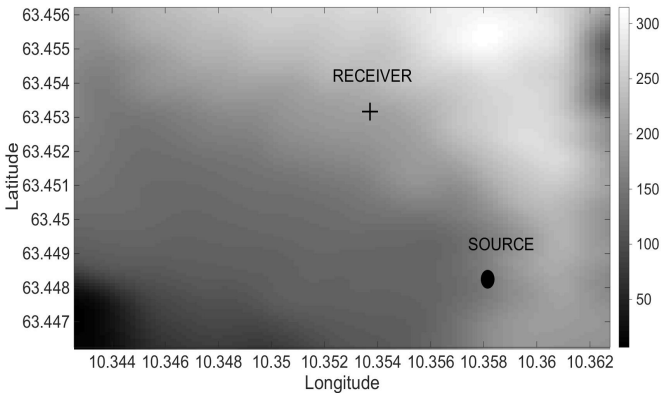

Figure 9: Bathymetry diagram of the TrondheimFjord region with source and receiver position. The source is shown by the circle and the receiver is shown by the cross. The depth at the source position is 150 m and depth at the receiver position is 200 m respectively. The source-receiver range is 480 m.

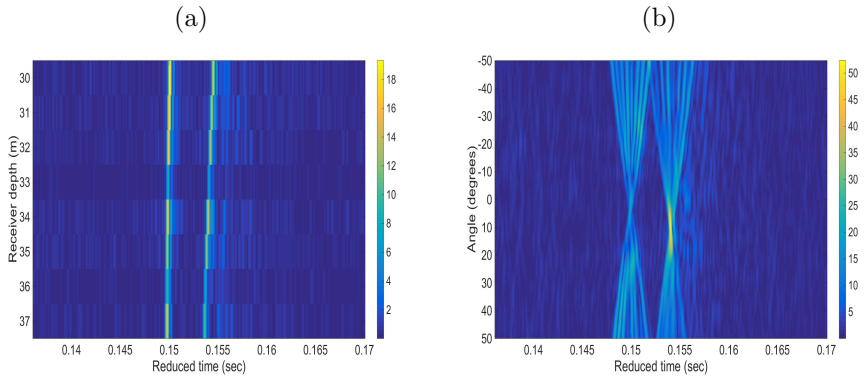

Figure 10: Characteristics of the channel for the experimental data. (a) The channel IR estimates along the receiver array, b) The beamforming results showing the angle of arrival.

with the spacing of 1 m between each element. The source was deployed at 50 m depth. The SSP was obtained at the receiver position and shown in Fig. 4.

Fig. 10 (a) shows the channel IR estimates at all eight hydrophones of the array. The figure is zoomed to show the first two arrivals. The first arrival reaches all the receiver at almost the same time which shows that it is the direct arrival. The second arrival reaches the bottom part of the array first. Fig. 10 (b) shows

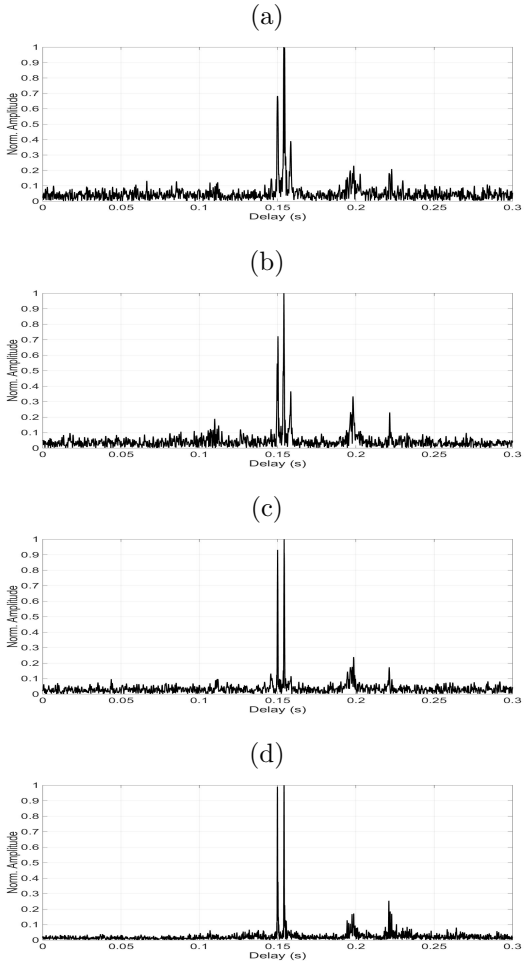

Figure 11: Channel IR estimates obtained from the experimental data at the fourth element of the array at 53 m depth. a) Channel IR obtained by "array weights 1", b) Channel IR obtained by "array weights 2", c) Channel IR obtained by "BF weights", d) Channel IR obtained by the pulse compression using the known LFM signal.

the beamforming results obtained from the channel IR estimates. The two arrivals reach the array at 7.7^o and 11.7^o.

Figs. 11 (a)-(c) show the channel IR computed by "array weights 1", "array weights 2" and "BF weights" respectively. Fig. 11 (d) shows the channel IR computed by the pulse compression using the known LFM signal. All the channel IR estimates are computed at the fourth element of the array at 53 m depth.

(a)

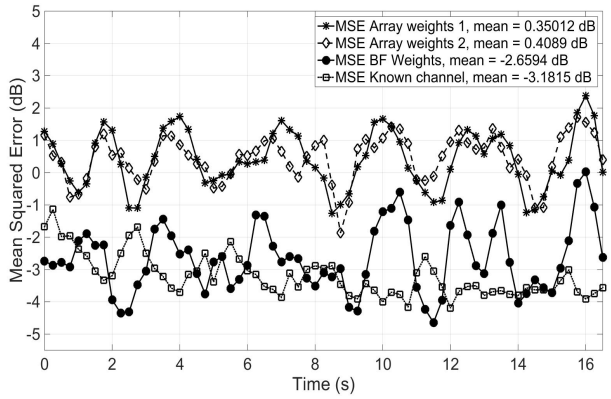

(b)

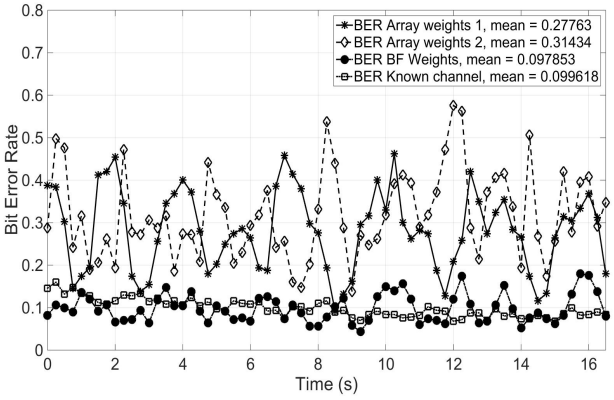

Figure 12: Performance comparison of different weighting function as a function of time for real data obtained during the experiment in the TrondheimFjord in Sept. 2017.

There are multiple arrivals reaching the receiver. In case of "array weights 1" and "array weights 2" there is extra arrival in the channel IR at 0.158 s. The arrival pattern obtained by the BF weights technique matches with the arrival pattern obtained by pulse compression.

290 Fig. 12 (a) shows the performance comparison in terms of MSE for different weighting techniques and the "known channel" case. Both the constant array weighting techniques, "array weights 1" and "array weights 2", provides mean MSE of 0.35 dB and 0.4 dB respectively. The BF-based weighting tech-

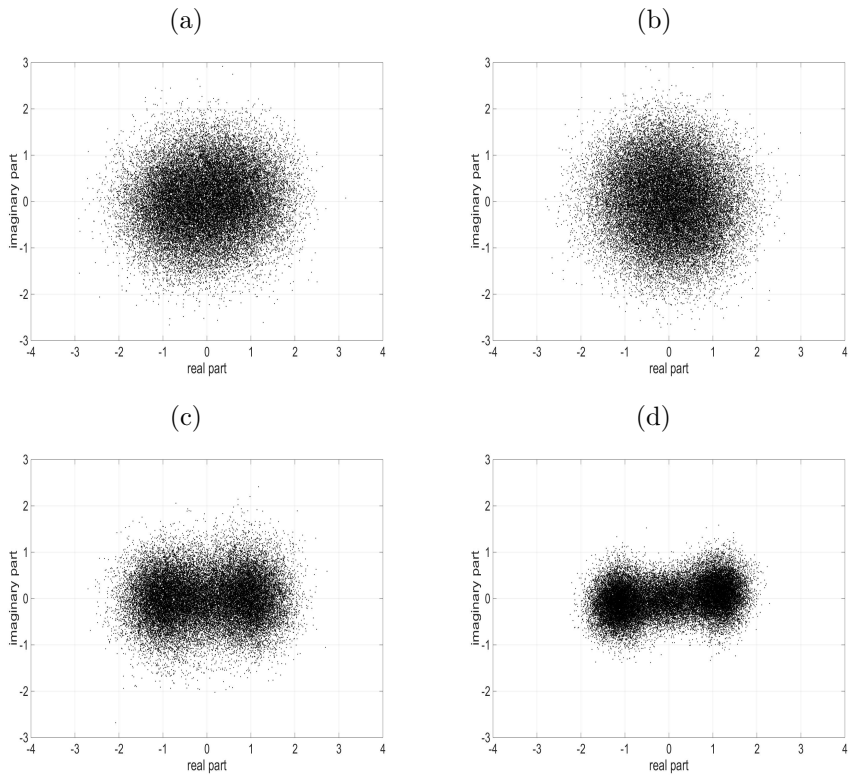

Figure 13: Constellation diagrams for different cases, (a) Array weights 1, (b) Array weights 2, (c) BF weights, (d) Known channel

nique performs better and gives a mean MSE of -2.65 dB. The performance of the known channel gives mean MSE of -3.18 dB. There is a difference of 0.53 dB between the BF weights and known channel case and the BF weighting technique outperforms the known channel at few instants. This is because the channel IR estimates are obtained from the probe signal which is transmitted before the data signal and the underwater channel varies during the data transmission. Fig. 12 (b) shows the performance comparison in terms of BER for different weighting techniques and the "known channel" case. The mean BER for "array weights 1" and "array weights 2" are 0.27 and 0.31 respectively. The performance in terms of BER for BF-based weighting technique and the known channel case are 0.098 and 0.099 respectively.

Fig. 13 shows the constellation diagram for different cases. Figs. 13 (a) and (b) show the constellation diagram in the case of "array weights 1" and "array weights 2". The performance is not good as the constellation appears a single cloud. Fig. 13 (c) shows the constellation diagram for the case of "BF weights" where the performance improves. Fig. 13 (d) shows the constellation diagram for the "known channel" case. For all the four cases, the phase rotation is compensated by using a known M-sequence.

5. Conclusions

In this work, a blind deconvolution based equalizer is proposed which uses the received array signal for channel IR estimation. These channel IR estimates are used for equalizing the effects of the channel. The channel estimation is done by applying different weighting functions to the received signal. The performance of different weighting functions is studied in terms of MSE and BER. The proposed equalizer is tested with simulated as well as real data. In both simulations and experimental results, the BF-based weights give better performance than the constant array weights. In addition to that, the performance of the BF-based weights is very close to the 'known channel" case which shows that BF-based technique provides good channel estimates and it can be used for blind channel estimation and equalization.

The main advantage of the proposed system is that it computes the channel estimates from the received array signal. This feature is very important for communications in different underwater applications including sensor networks and underwater vehicles. For underwater sensor networks, it can save the resources allocated for channel estimation which will result in longer battery time. For underwater vehicles, the underwater channel is changing very fast and in such scenarios, the blind channel estimation techniques will be very beneficial. In this work, the proposed method is tested for a static environment and future work will involve testing it in a time-varying environment.

References

[1] D. Kilfoyle, and A.Baggeroer, The state of the art in underwater acoustic telemetry, IEEE J. Ocean. Eng. 25, no. 1 (2000) 4–27.

[2] M. Stojanovic, J. A. Catipovic, J. G. Proakis, Phase-coherent digital communications for underwater acoustic channels, IEEE Journal of Oceanic Engineering 19 (1) (1994) 100–111.

[3] O. Hinton, G. Howe, and A. Adams, An adaptive high bit rate sub-sea communications system, Proceeding of European Conference on Underwater Acoustics, Bressels, Belgium (1992) 75–79.

[4] M. Suzuki, and T. Sasaki, Digital acoustic image transmission system for deep sea research submarsible, Proceeding of Oceans '92, Newport, RI (1992) 567–570.

[5] J. Fischer, K. Bennet S. Reible J. Cafarella and I. Yao, A high rate underwater acoustic data communication transceiver, Proceeding of Oceans '92, Newport, RI (1992) 571–576.

[6] G. Sandsmark, A. Torsvik and J. Hovem, Shallow water coherent acoustic data transmission, Proceeding of European Conference on Underwater Acoustics, Bressels, Belgium (1992) 88–91.

[7] J. Proakis, Digital Communications, McGraw-Hill, New York,, 1989.

[8] M. Stojanovic, J. Catipovic and J. Proakis, Coherent communications over long range acoustic telemetry channels, NATO ASI Series on Acoustic Signal Processing for Ocean Exploration (1993) 607–612.

[9] W. A. Kuperman, W. S. Hodgkiss, H. C. Song, T. Akal, C. Ferla, D. R. Jackson, Phase conjugation in the ocean: Experimental demonstration of an acoustic time-reversal mirror, The Journal of the Acoustical Society of America 103 (1) (1998) 25–40.

[10] G. Edelmann, W. Hodgkiss, S. Kim, W. Kuperman, H. Song, T. Akal, Underwater acoustic communication using time reversal, in: OCEANS, 2001. MTS/IEEE Conference and Exhibition, Vol. 4, 2001, pp. 2231 –2235 vol.4.

[11] M. Stojanovic, J. Catipovic, and J. G. Proakis, Reduced-complexity multi-channel processing of underwater acoustic communication signals, J. Acoust. Soc. Am. 98 (1995) 961–972.

[12] J. C. Preisig, Performance analysis of adaptive equalization for coherent acoustic communications in the time-varying ocean environment, The Journal of the Acoustical Society of America 118 (1) (2005) 263–278.

[13] António João Silva, Environment based underwater communications, PHD Dissertation University of Algarve.

[14] U. Vilaipornsawai, A. J. Silva and S. M. Jesus , Underwater communications for moving source using geometry-adapted time reversal and dfe: Uan10 data, in: OCEANS 2011 IEEE Conference, Santandar, Spain, 2011, pp. 1–7.

[15] N. E. Martins, S. M. Jesus, Blind estimation of the ocean acoustic channel by time frequency processing, IEEE Journal of Oceanic Engineering 31 (3) (2006) 646–656.

[16] W.-J. Zeng, X. Jiang, X.-L. Li, X.-D. Zhang, Deconvolution of sparse underwater acoustic multipath channel with a large time-delay spread, The Journal of the Acoustical Society of America 127 (2) (2010) 909–919.

[17] G. B. Smith, Multipath compression by multiple convolutions, The Journal of the Acoustical Society of America 113 (4) (2003) 2213–2213.

[18] K. G. Sabra, D. R. Dowling, Blind deconvolution in ocean waveguides using artificial time reversal, The Journal of the Acoustical Society of America 116 (1) (2004) 262–271.

[19] S. H. Abadi, D. Rouseff, D. R. Dowling, Blind deconvolution for robust signal estimation and approximate source localization, The Journal of the Acoustical Society of America 131 (4) (2012) 2599–2610.

[20] Finn B. Jensen, William A. Kuperman, Micheal B. Porter and Henrik Schmidt, Computational Ocean Acoustics, American Inst. of Physics, 2000.

[21] M. Porter, E. L. Reiss, A numerical method for oceanacoustic normal modes, The Journal of the Acoustical Society of America 76 (1) (1984) 244–252.

[22] A. Silva, O. Rodriguez, F. Zabel, J. Huilery, and S. M. Jesus, Underwater acoustics simulations with time variable acoustics propagation model, Proceeding of 10th European Conference on Underwater Acoustics 2 (2010) 989–996.